Northumbria Research Link

This version was downloaded from Northumbria Research Link: http://nrl.northumbria.ac.uk/id/eprint/43676/

Northumbria University NEWCASTLE

University**Library**

Ultrafast and Sensitive Self-Powered Photodetector Featuring Self-Limited Depletion Region and Fully-Depleted Channel with van der Waals Contacts

Mingjin Dai[†,‡], Hongyu Chen[‡], Fakun Wang[#], Mingsheng Long[§], Huiming Shang[‡], Yunxia Hu[†,‡], Wen Li[†,‡], Chuanyang Ge[‡], Jia Zhang[‡], Tianyou Zhai[#], Yongqing Fu[&], and PingAn Hu*[†,‡]

[†]School of Materials Science and Engineering, [‡]MOE Key Laboratory of Micro-Systems and Micro-Structures Manufacturing, Harbin Institute of Technology, Harbin 150001, P. R. China. [#]State Key Laboratory of Material Processing and Die and Mould Technology, School of Materials Science and Engineering, Huazhong University of Science and Technology, Wuhan 430074, P. R. China. [§]Institutes of Physical Science and Information Technology, Anhui University, Anhui, 230601, P. R. China. [&]Faculty of Engineering & Environment, Northumbria University, Newcastle upon Tyne, NE1 8ST, UK. *E-mail: hupa@hit.edu.cn.

ABSTRACT: Self-powered photodetectors with great potentials for implanted medical diagnosis and smart communications, have been severely hindered by the difficulty of simultaneously achieving high sensitivity and fast response speed. Here, we report an ultrafast and highly sensitive self-powered photodetectors based on two-dimensional (2D) InSe, which is achieved by applying a device architecture design and generating ideal Schottky or ohmic contacts on 2D layered semiconductors, which are difficult to realize in the conventional semiconductors owing to their surface Fermi-level pinning. The as-fabricated InSe photodiode features a maximal lateral self-limited depletion region and a vertical fully-depleted channel. It exhibits a high detectivity of 1.26×10^{13} Jones and an ultrafast response speed of ~200 ns, which breaks the response speed limit of reported self-powered photodetectors based on 2D semiconductors. The high sensitivity is achieved by an ultralow dark current noise generated from the robust van der Waals (vdWs) Schottky junction and a high photoresponsivity due to the formation of maximal lateral self-limited depletion region. The ultrafast response time is dominated by the fast carrier drift driven by a strong build-in electric field in the vertical fully-depleted channel. This device architecture can help us to design high-performance photodetectors utilizing vdWs layered semiconductors.

KEYWORDS: two-dimensional semiconductor, van der Waals contacts, fully depleted channel, self-limited depletion region, nanoseconds

Owing to their unique structural, physical, electrical and optical properties, 2D layered materials and their vdW heterostructures have recently attracted considerable attention in the field of photodetectors.[1-6] However, poor detectivity and slow response speed hinder their successful applications. To overcome these drawbacks and improve the sensitivity, researchers developed two different strategies: improving quantum efficiency, or suppressing dark currents. Different methods have been proposed to improve the quantum efficiency of the photodetectors: i) enhancing light absorption by introducing light absorbing media;[7-14] ii) increasing separation of photon-generated electrons and holes,[15-19] iii) improving gain of photocurrents with trapping effect and avalanche effect.[20,21] On the other hand, the dark current can be suppressed by generating energy barrier formed by dielectrics insertion,[22] band-gap engineering,[23-25] and regional doping.[26] A fast response speed of photodetectors is important for practical applications such as fast imaging, ultrafast dynamic process monitoring, and high-speed optical communication.[27] Most of the existing photodetectors based on 2D semiconductors exhibit a long response time ranging from milliseconds to dozens of seconds due to their long carrier lifetimes, low mobility and long device channels.[12] Therefore, a crucial issue for the next generation 2D semiconductor based photodetectors is to explore the suitable strategy to achieve both high detectivity and fast response speed, and this includes those of photovoltaic detectors (also called self-powered photodetectors). For examples, the response times for most of reported self-powered photodetectors based on 2D semiconductors are ranged from microseconds to milliseconds,[28,29] even though it is believed that these photovoltaic devices based on *p-n* diodes or Schottky diodes usually possess better high-frequency characteristics than those of the photoconductive devices.[30]

For the self-powered photodetector, the depletion region plays a significant role in photodetection due to its significant influence of carriers separation and transport. Generally, the larger depletion region exposed to the illumination can generate more carriers effectively, and also increase the carrier transit time in a lateral *p-n* homo/hetero junction or a Schottky diode device.[25,31-34] In the cases of the commonly investigated vertical photodiode devices, the carriers' diffuse time in the lateral direction and out of the depletion region limits the response speed, although the carriers can be separated and then drift under the build-in electric field in the vertical direction (Figure S1,Supporting Information).[35-37] On the other hand, the metal contacts have significant effect on the depletion region. For the conventional semiconductors, it is difficult to realize ideal Schottky or ohmic contacts owing to the surface Fermi-level pinning, whereas the near-perfect surfaces of 2D semiconductors can make that come true through forming vdWs contacts.[38-40]

In this work, we reported a vertical InSe photodiode with asymmetric vdWs contacts that features a maximal lateral self-limiting depletion region and a vertical fully-depleted channel to achieve both ultrafast response speed and ultrahigh sensitivity. Owing to the unilateral depletion region arising from the perfect vdWs ohmic contact at graphene(Gr)-InSe interface and the robust metal Schottky contact at Au-InSe interface, this Schottky diode exhibits an excellent rectifying characteristic with a rectification ratio over 10^4. Upon the light illumination, a large amount of carriers generated in the self-limiting depletion region transit to the Gr electrode driven by the large build-in electric field rapidly, thereby allowing an ultrahigh sensitivity and a super-short response time of sub-microseconds simultaneously. As based on the synergistic effect of lateral self-limiting depletion region and strong build-in electric field, the distinctive Au/InSe/Gr Schottky diode exhibits a low noise of 1-2 fA/Hz$^{1/2}$ and a high responsivity of 365

mA/W, yielding an ultrahigh detectivity of 1.26×10^{13} Jones. In addition, an ultrafast response speed of ~200 ns is achieved, which, to the best of our knowledge, is faster than most reported self-powered photodetectors based on 2D semiconductors.[41]

RESULTS AND DISCUSSION

To achieve high-performance self-powered photodetector, vdWs layered InSe nanosheets with over 50 nm thickness, which possess a high optical absorption coefficient ($> 10^6$ cm^{-1}) because of its direct bandgap of 1.25 eV, and a high electron mobility ($> 10^3$ cm^{2}V^{-1}s^{-1}), were used as the active materials.[4,42,43] The InSe nanosheets exfoliated from a bulk crystal were characterized firstly with a high-resolution transmission electron microscope (HR-TEM), and the hexagonal patterns in the selective area electron diffraction image and lattice fringes in the HR-TEM images indicate the highly crystalline InSe nanosheet (Figure S2, Supporting Information). Figure 1a shows the device architecture of vertical InSe Schottky diode, where a multilayer Gr was used as bottom electrode and the gold layer was used as the top electrode. A typical optical image of the vertical InSe device is shown in Figure 1b. The thickness of InSe nanosheet is about 110 nm (Figure S3, Supporting Information). Raman spectrum of the vertical InSe/Gr heterostructure shown in Figure 1c exhibits five peaks located at 115, 176, 228, 1589 and 2721 cm^{-1}, which are consistent with the A^1_{1g}, E^1_{2g}, and A^2_{1g} phonon modes of β-InSe and G and 2D phonon modes of Gr, respectively.[32,44] Furthermore, the Raman mapping image demonstrates the device structure and reveals the interface coupling between InSe and Gr, which can be confirmed from the obvious Raman quenching effect in the overlapping region as shown in Figures 1d and 1e.[45]

As the first step to achieve an InSe Schottky diode, two asymmetric vdWs contacts were set to be Au and Gr based on their energy band structures (Figure S4, Supporting Information). The Fermi level of InSe nanosheet is higher than that of Gr indicating an ohmic contact for the bottom electrode.[46] To provide more evidences that the ohmic contact is formed between Gr and InSe, photoluminescence (PL) measurements of both the isolated InSe and InSe/Gr heterostructure were conducted (Figure S5a, Supporting Information). The strong PL peak located at 1.25 eV matches well with the bandgap of InSe nanosheet. As for the InSe/Gr heterostructure, there is a dramatic PL quenching with a 46% reduction, which demonstrates that some of photo-induced carriers recombine through a non-radiative way rather than a radiative way, along with a charge transfer from InSe to Gr.[25,47] In addition, the transient PL studies were performed to validate the charge transfer at the InSe-Gr interface (Figure S5b, Supporting Information). By fitting the transient PL decay curves, the carrier lifetimes (τ) for isolated InSe and InSe/Gr heterostructure are $\tau_{InSe}=0.284$ and $\tau_{InSe/Gr}=0.265$ ns, respectively. The fluorescence decay rate ($1/\tau_{InSe/Gr}$) of InSe/Gr heterostructure can be expressed as: $1/\tau_{InSe/Gr} =1/\tau_{InSe} +1/\tau_{CT}$, where τ_{CT} is the charge transfer time from InSe to Gr.[48,49] The charge transfer time can be calculated to be 3.961 ns. Thus, it can be concluded that the photo-induced electrons will be transferred to Gr much faster, driven by the band bending of InSe nanosheet, and then recombine with holes through a non-radiative way (Figure S5c, Supporting Information).[22] These results verify a higher Fermi level of InSe than that of Gr and indicate a vdWs ohmic contact of Gr with InSe. In order to provide experimental demonstration of ohmic contact for Gr and InSe, the InSe device with two Gr electrodes was fabricated as shown in Figure S6 in the Supporting Information. The linear I_{ds}-V_{ds} curves obtained both under dark and light illumination reveal the ideal ohmic contact of the Gr-InSe-Gr device, which offer us to achieve a perfect ohmic contact

in the vertical InSe Schottky diode. In the case of Schottky contact of Au with InSe, the I_{ds}-V_{ds} curves of two-terminal Au-InSe-Au device show non-linear behaviors indicating a Schottky contact (Figure S7, Supporting Information). These results are consistent with our and other previous reports.[32, 46]
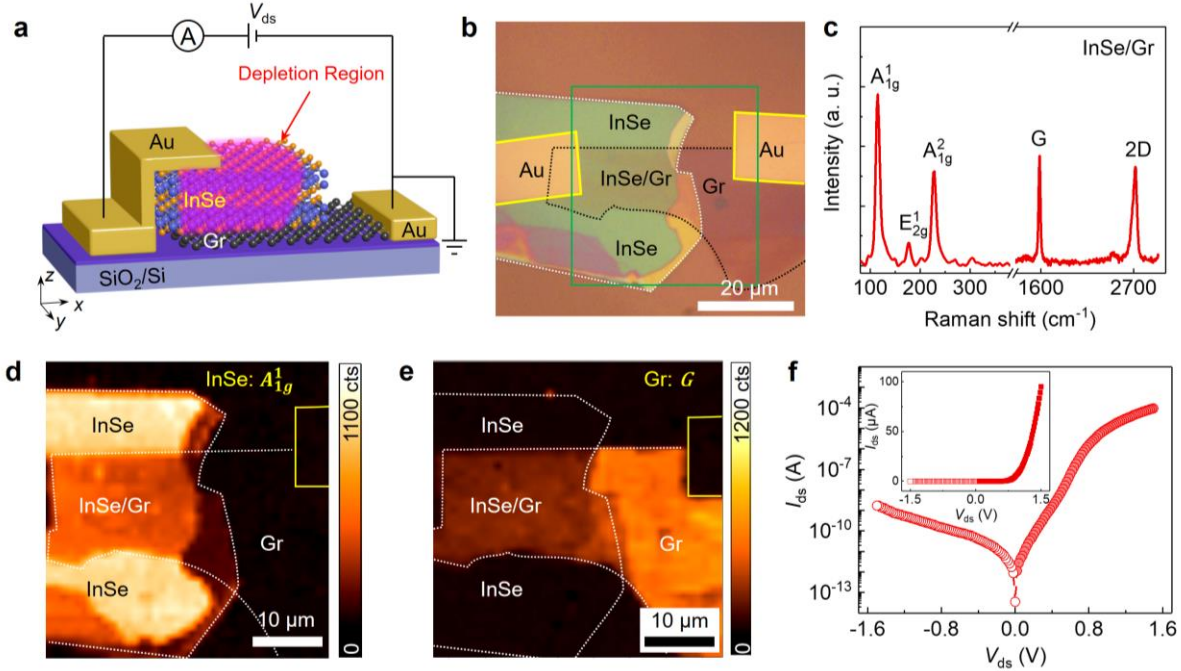
Figure 1. Device architecture, characterization, and electron transport properties of the vertical InSe Schottky diode. (a) Schematic device structure of the InSe Schottky diode. (b) Optical image of the vertical InSe Schottky diode device. (c) Raman spectrum of InSe/Gr heterostructure. (d) Raman mapping image of A_{1g}^1 mode for InSe. (e) Raman mapping image of G mode for Gr. (f) I_{ds}-V_{ds} characteristics of an InSe Schottky diode. Inset: the same I_{ds}–V_{ds} curve in a linear scale.

Based on above results about the contact type of both Au and Gr with InSe, the vertical Au-InSe-Gr device is expected to be a Schottky diode with a robust vdWs Schottky contact and a perfect vdWs ohmic contact simultaneously. The I_{ds}-V_{ds} curves of vertical Au-InSe-Gr device exhibits a standard rectification behavior as a regular Schottky diode as shown in Figure 1f. The rectification ratio is over to 3.2×10^4 at $|V_{ds}|$=1.5 V. Considering the nanoscale channel in the vertical InSe Schottky diode, the dominated carrier transport may be direct tunneling (DT) *via*

field emission or Fowler−Nordheim tunneling (FNT), which is evidenced by the replotted I_{ds}-V_{ds} curve (Figure S8, Supporting Information). By modeling the I_{ds}-V_{ds} curve with the DT and FNT at lower and higher biases, the tunneling barriers can be estimated to be 0.605 eV and 0.101 eV for the Au and Gr contact, respectively. These results further demonstrate that a robust vdWs Schottky junction is formed at the Au-InSe interface, while an ideal vdWs ohmic junction is formed at the Gr-InSe interface, thereby fabricating a vertical InSe Schottky diode with a unilateral depletion region successfully.

To evaluate the photovoltaic detection performance of the vertical InSe Schottky diode, the photoelectric characterizations were conducted as shown in Figure 2a. An obvious photovoltaic effect can be observed when the vertical InSe Schottky diode is illuminated by the light with various wavelengths. The reliable and stable photoelectric responses under the light illumination demonstrate a good reliability (Figure S9, Supporting Information). Figure 2b shows the I_{ds}-V_{ds} curves under dark and 400 nm illumination with various luminous fluxes. Both the short-circuit current (I_{sc}) and open-circuit voltage (V_{oc}) increase with light power, which is increased from 0.08 to 8.36 nW. To further investigate the power dependent photo-responses of the vertical InSe Schottky diode in a self-powered mode, the power-dependent short-circuit current I_{sc} and responsivity were recorded and displayed in Figure 2c and Figure S10 in the Supporting Information. The short-circuit current I_{sc} exhibits an almost linearly dependent with the light power, which can be fitted by power law: $I_{sc} \propto P^{0.947}$, where P is the effective light power. The responsivity (R) can be calculated by $R = I_{sc}/P$. As a result, the responsivity is almost unchanged with the increase of light power and possesses a value of 350 ± 30 mA/W. In addition, based on the linear relation between short-circuit current I_{sc} and light power P, the open-circuit voltage V_{oc} exhibits a logarithmic relationship with the light power P (Figure S11, Supporting

Information).[41] Moreover, another important figure-of-merit for photodetector is linear dynamic range (LDR), which can characterize the light intensity range in which the photodetectors have a constant responsivity.[50] The LDR is described with decibels (dB) and can be calculated by: LDR=20 log (P_{sat}/P_{low}), where P_{sat} (P_{low}) is the light intensity stronger (weaker) than which the photocurrent begins to deviate from linearity. Here, for our device, the calculated LDR can over to 40 dB according to the results shown in Figure 2c.

As a crucial parameter to evaluate the capability of photodetector to detect weak radiation, the detectivity is defined as $D^* = (AB)^{1/2}/NEP$, where A is the device area, B is the electrical band-width of the channel, and NEP denotes the noise equivalent power, which can be calculated by the expression: NEP=i_n/R (i_n is the dark current noise). Generally, the dark current noise i_n consists of shot noise, thermal noise, and flicker noise (or 1/f noise).[50] To fully consider the frequency-dependent noise, the current noise of the vertical InSe Schottky diode was recorded at zero bias using a lock-in amplifier and a low-noise preamplifier (Figure 2d). Interestingly, the noise current shows a linear dependence on the frequency with a 1/f slope in the low frequency (<1 kHz), whereas it is almost unchanged with an ultralow value of ~1 fA/Hz$^{1/2}$ when the frequency is over 1 kHz. This demonstrates that the current noise is dominated by the flicker noise at lower frequencies, and the white noise (including shot noise and thermal noise) at higher frequencies. In addition, the current noise keeps in a low level even under a low reverse bias (Figure S12, Supporting Information). The ultralow noise level at high frequencies may be due to the ultralow dark current caused by the robust Schottky barrier, indicating a high sensitivity of the vertical InSe Schottky diode. Based on the small noise current, the D^* of the device can reach 1.26×10^{13} Jones under the 400 nm light illumination. To further investigate spectral detection range of the vertical InSe Schottky diode, the spectral responses of both responsivity

and detectivity are measured and shown in Figure 2e. The device can detect the radiation in the wavelength range from UV to near-IR, and possesses a cut-off wavelength of around 1000 nm arising from the bandgap 1.25 eV of InSe. The rapid and reproducible photo-switching responses under multiple periodic on/off laser illuminations imply a good stability of our device (Figure S13, Supporting Information).
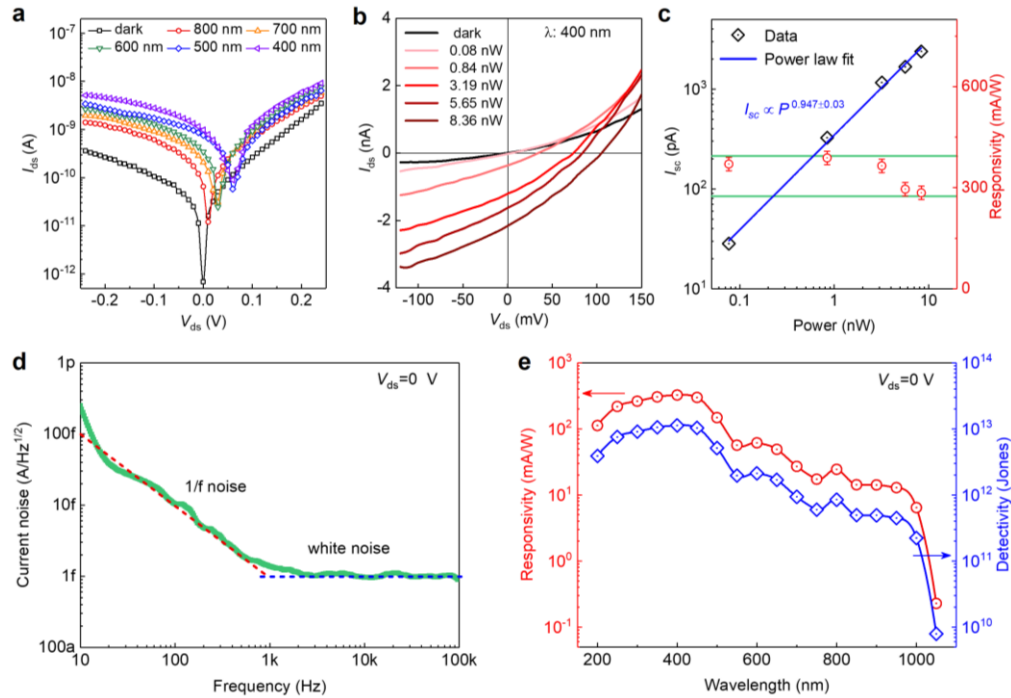
Figure 2. Photovoltaic detection performance of the vertical InSe Schottky diode. (a) I_{ds}–V_{ds} curves of the vertical InSe Schottky diode under dark and laser illumination with various wavelength. (b) The light power dependent I_{ds}–V_{ds} curves under 400 nm light illumination. (c) Light power dependent shor-circuit current I_{sc} and responsivity. (d) Current noise of the InSe photodiode at V_{ds}= 0 V. (e) Self-powered spectral responses of responsivity and detectivity at a high frequency (> 1 kHz).

Apart from the detectivity, the response speed is also a very important figure-of-merit for photodetectors. Generally, the response speed dominates the 3 dB bandwidth ($f_{-3\,dB}$), which is effected by both the charge-carrier transit time (t) and resistance-capacitance (RC) constant, and can be expressed by: $f_{-3\,dB}^{-2} = (3.5/2\pi t)^{-2} + (1/2\pi RC)^{-2}$. The 3 dB bandwidth $f_{-3\,dB}$ denotes a cut-off frequency of modulated incident light at which the photocurrent signals are attenuated to 70.7%

of its initial value.[51,52] Here, the response time of our device was measured by a transient photocurrent (TPC) technique using a pulse 532 nm laser with 8 ns plusewidth and an oscilloscope with a 50 Ω input resistor (Figure S14, Supporting Information). Figure 3a shows the recorded TPC curves under zero bias with the periodic laser illumination at a frequency of 2 kHz. By fitting the monoexponential TPC decay curve, the response time of our device is 235 ns as shown in Figure 3b, which was the fastest response speed reported for all the current 2D semiconductor based self-powered photodetectors. Apparently, the photovoltaic detector possesses a faster response speed than that of the InSe based photoconductive detector with ohmic contact or Schottky contact (Figure S6 and S7, Supporting Information), In addition, the response speed of vertical InSe Schottky diode is about three orders of magnitude faster than that of the lateral InSe Schottky photodiode (Figure S15, Supporting Information). The lateral InSe Schottky diode with a longer lateral channel can be equivalent to a photodiode and a series resistor. As a result, the control device exhibits an obvious photovoltaic behavior under light illuminations, while possesses a much slow photoresponse speed with a response time of 107.1 μs.

To determine whether the charge-carrier transit time t or the RC time constant dominates the response speed in our device, we firstly study the RC time constant by calculating the width of depletion region (W_D). For the Sckotty diode, the depletion region capacitance C_D of metal-semiconductor junction can be calculated by: $C_D = \varepsilon_s/W_D$, where ε_s is the dielectic constant of semiconductor. The width of depletion region W_D can be estimated by: $W_D = ((2\varepsilon_s/qN_D) \times (\varphi_{bi} - V - kT/q))^{1/2}$, where q is the element charge, k is the Boltzmann constant, T is the temperature, φ_{bi} is the build-in potential, V is the applied bias, and N_D is the carrier concentration of semiconductor, which can be obtained by Hall measurement for InSe nanosheet (Figure S16, Supporting

Information). Based on the calculated depletion region width W_D of 6.7 μm, the depletion region capacitance C_D of our device is several pF and the RC time constant is estimated to be lower than 1 ns, which is far shorter than the measured response time.[50] Therefore, we can conclude that the response speed of our vertical InSe Schottky diode device is dominated by the charge-carrier transit time.

Next, the laser power-dependent response time measurements provide more experimental evidence that the response speed is limited by the charge-carrier transit time in our device. Figure 3c displayed that the laser power dependent response time and the shortest response time can reach 167 ns as shown in Figure S17 in the Supporting Information. Interestingly, the response time decreases as the laser power is increased because of the enhanced diffusion of carriers induced by the improved photo-generated carrier concentration.[50] However, the response time increases as the laser power is further increased due to the attenuation of build-in electric field screened by photo-generated space-charges.[51,53]
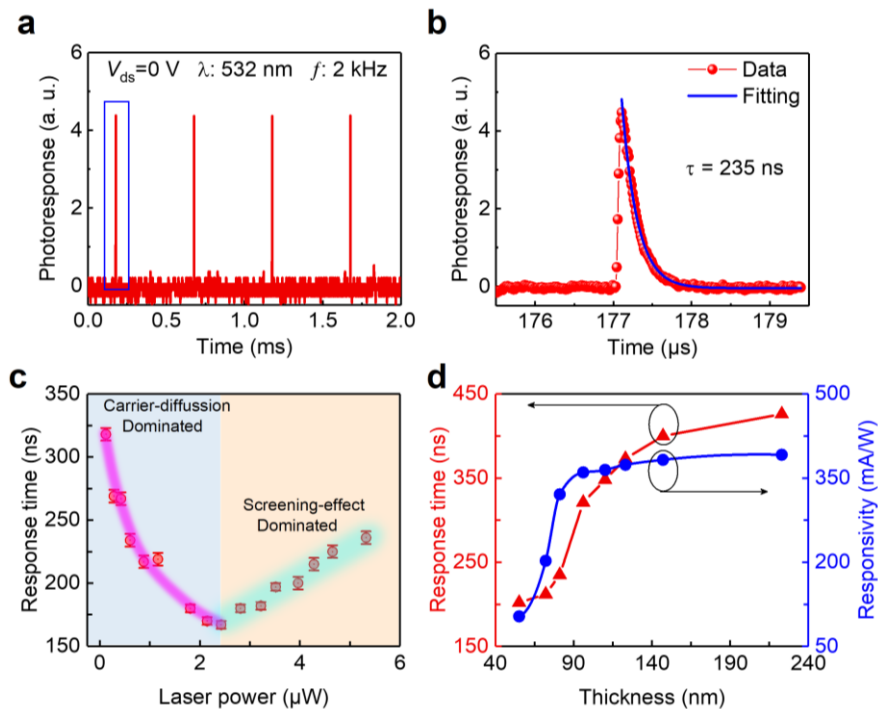
Figure 3. Transient photoresponse of the InSe Schotty diode. (a) Transient photoresponse signals recorded in photovoltaic mode. (b) A typical signal fitted with a monoexponential decay function. The extracted response time is about 235 ns. (c) Laser power dependent response times dominated by carrier-diffussion or screening-effect in the depletion region. (d) InSe thickness dependent response time and responsivity.

Furthermore, effect of InSe nanosheet thickness on the response time was also investigated. Seven devices with different InSe thicknesses were fabricated and are displayed in Figure S18 in the Supporting Information. The corresponding TPC curves were recorded (Figure S19, Supporting Information) and the extracted response time as a function of InSe thickness is shown in Figure 3d. The thicker the InSe nanosheet used, the longer response time of the vertical Schottky diode is, which verifies again that the charge-carrier dominates the response time in our devices. The same variation of response time with laser power can also be observed in the vertical InSe Schottky diodes with different InSe thicknesses (Figure S20, Supporting Information). Besides the response time, the responsivity is also affected by the thickness of InSe nanosheet. As shown in Figure 3d, the responsivity is increased with the InSe thickness and then saturated to be around 400 mA/W, which may be because the incident radiation is mostly absorbed by the top InSe layers owing to its high light absorption efficiency. Nevertheless, all these devices still possess ultrafast response speeds with the response times ranging from 200 to 450 ns and high responsivity values ranging from 60 to 400 mA/W, which are better than or comparable to most reported self-powered photodetectors based on 2D semiconductors (Table S1, Supporting Information).

As stated above, the depletion region at the junction is pivotal for the self-powered photodetection in photodiode devices. To facilitate direct observation of the depletion region in our device, the spatial distributions of potential, electrons, and holes concentration were simulated using finite element method (FEM) with COMSOL Multiphysics software. Figure 4a shows the top view of the potential distribution of our vertical InSe Schottky diode under a zero

bias. A self-limited depletion region with gradient potential is limited around the Au contact in InSe nanosheet due to the non-uniform distribution of electron and hole at the junction (Figure S21, Supporting Information). From the potential profile as shown in Figure 4b, the self-limited depletion region can be as large as ~6.5 μm, which is in good accordance with the calculated depletion region width of 6.7 μm. Furthermore, the depletion region can be extended when the device is under a reverse bias of V_{ds}= -0.1 V because of the increased non-uniform distribution of carriers (Figure S22, Supporting Information).
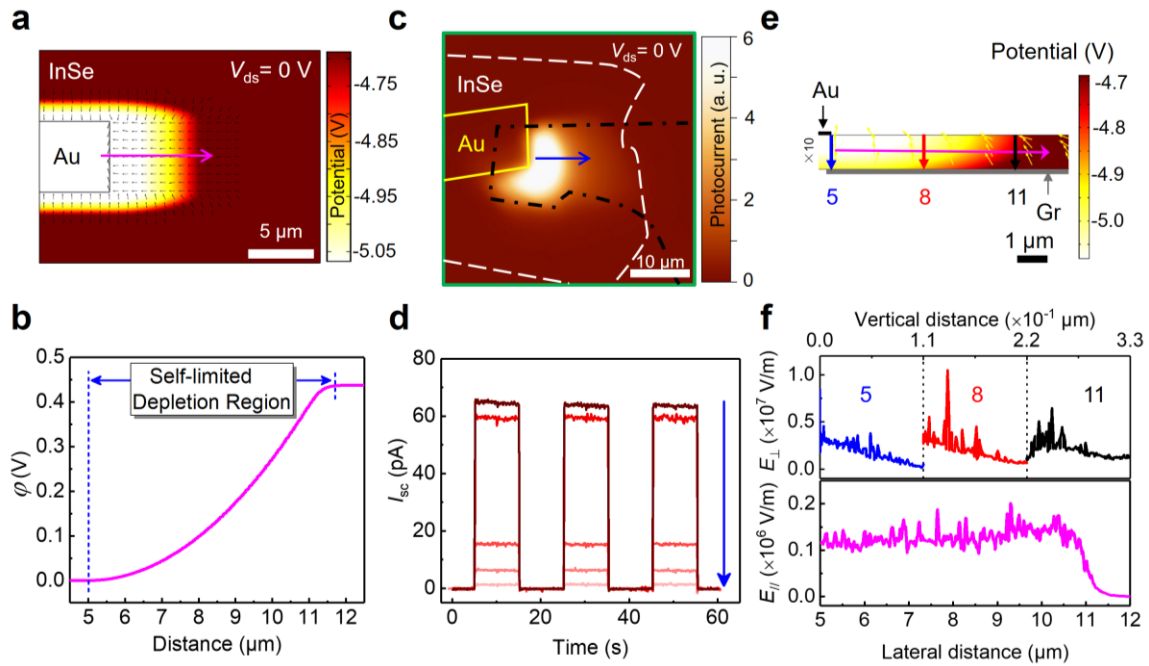
Figure 4. Lateral self-limited depletion region and vertical fully depleted channel in the InSe Schottky diode. (a) The simulated lateral potential distribution of the device under a zero bias. (b) The potential profile along the arrow labelled in Figure 4a. (c) The photocurrent mapping image of the device under a zero bias. (d) Corresponding linear scanning of short-circuit current I_{sc} along the blue line labelled in Figure 4c. (e) The simulated vertical potential distribution of the device under a zero bias. (f) The build-in electric field profiles along both lateral ($E_{//}$) and vertical ($E_{\perp}$) directions.

In order to determine that the self-limited depletion region dominates the photo-responses in our device, the photocurrent mapping was measured (Figure S23, Supporting Information). As shown in Figure 4c and Figure S23 in the Supporting Information, the major photocurrents obtained at zero bias are located around the Au electrode, and the photocurrents decrease

dramatically away from the junction, which can be found from the linear photocurrents scanning (Figure 4d). These indicate that the self-limited depletion region at Schottky junction dominates the generation of photocurrent in our device. In addition, the extended photocurrent distribution under a reverse bias (Figure S24, Supporting Information) further demonstrates that the photocurrent generation is attributed to the lateral depletion region, which matches well with the FEM simulated result. Based on these results, it can be concluded that the large lateral self-limited depletion region indeed dominates the photocurrent generation in the vertical InSe Schottky diode, thereby resulting in high responsivity and high detectivity.

On the other hand, understanding the mechanism of ultrafast photo-responses of the vertical InSe Schottky diode is important for interpreting experimental results. This can be explained by the ultrafast carrier drift in the self-limited depletion region, because the carrier diffusion time given by the well-designed device architecture as stated above can be considered negligible. The electron, hole, and potential distributions of our device were simulated in a side view to understand the effect of depletion region on the response speed (Figure S25, Supporting Information). Figure 4e shows the enlarged side view of spatial distribution of potential for the vertical InSe Schottky diode under zero bias. The yellow arrows show the build-in electric field in the self-limited depletion region. To facilitate the analysis about the carrier drift in the self-limited depletion region, the build-in electric field profiles along both lateral ($E_{//}$) and vertical ($E_{\perp}$) directions were plotted and are shown in Figure 4f. It is worth noting that the vertical scale of InSe thickness has been magnified ten times for enhancing visualization. For the vertical electric field $E_{\perp}$, it can reach up to about 4×10^6 V/m and decrease to zero at the bottom Gr electrode for different positions as shown in Figure 4e. In the case of lateral electric field $E_{//}$, it possesses an almost unchanged value of 0.12×10^6 V/m in the self-limited depletion region. As we all know,

the charge-carrier drift time (t_d) is related to the mobility (μ), electric field (E), and transport distance (L), and can be expressed as: $t_d = L/(\mu E)$. According to our and others' previous reports, the electron and hole mobilities of InSe at room temperature are 10^2-10^3 and 10^0-10^1 cm^2 V^{-1} s^{-1}, respectively.[4,46,54,55] Considering the lower hole mobility in InSe nanosheet, the carrier drift time will be dominated by the hole drift time in the self-limited region. As a result, the carrier drift time can be estimated to be 60-600 ns in the lateral direction and 0.05-0.5 ns in the vertical direction. These calculated results match well with our experimental results for the response time, indicating that the response time is indeed dominated by the carrier drift in the self-limited depletion region.

Overall, the device operation mechanism of the vertical InSe Schottky diode can be illustrated as shown in Figure 5a. As discussed above, a large lateral self-limited depletion region and a fully depleted channel was formed due to the robust Schottky junction of Au contact. This Schottky barrier not only suppresses the dark current noise, but also provides sufficient effective illumination area for high efficient optoelectronic conversion. For the photodetection process, firstly, vast electron-hole pairs will be excited by the incident light and separated quickly by the strong build-in electric field within 300 ps according to the transient PL measurements (Figure S5, Supporting Information).[56,57] Then the photo-induced holes and electrons were swept out to top Au electrode and bottom Gr electrode, respectively. This step will take hundreds of nanoseconds owing to a relative low hole mobility of InSe, which was demonstrated by both the TPC measurements and theoretical calculations as previously mentioned (Figure 3 and Figure 4).
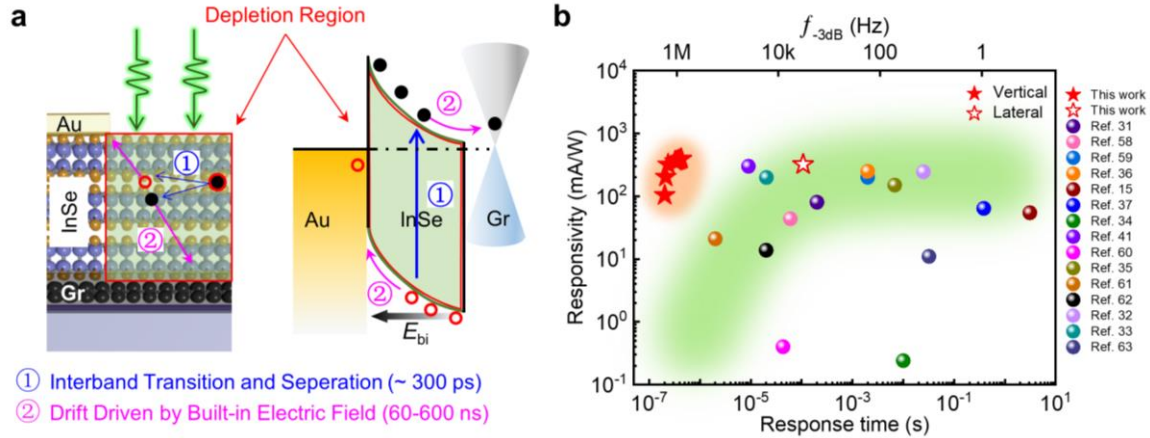
Figure 5. Working mechanism and performance comparison. (a) Illustration of photodetection mechanism and dynamic process of photo-induced carriers in the vertical InSe Schottky diode. (b) Performance summary of 2D semiconductors based self-powered photodetectors.

We further proved the superiority of our vertical InSe Schottky diode for ultrafast self-powered photodetection by comparing its performance with the previously reported 2D based self-powered photodetectors. As shown in Figure 5b, our vertical InSe Schottky diode exhibits excellent self-powered photodetection performance including the comparable responsivity and the fastest response speed compared with other reported results (Table S1, Supporting Information).[15,31-37,41,58-63] Therefore, we can conclude that the vertical InSe Schottky diode with well-designed device architecture is a potentially superior candidate for self-powered ultrafast photodetection.

CONCLUSIONS

In summary, we proposed a vertical InSe Schottky diode featuring a self-limited depletion region with a large lateral scale and a vertical nanoscale. The photodiode exhibits an ultralow dark current noise given by the robust Schottky barrier and a high responsivity supported by the large lateral depletion region. As a result, an ultrahigh sensitivity was realized by achieving a high detectivity of 1.26×10^{13} Jones. More importantly, based on the strong build-in electric field

induced by the self-limited depletion region, the photodiode exhibits a record ultrafast response speed with a sub-microsecond response time. In addition, the performance of this kind of Schottky photodiodes could be further improved through increasing Schottky barrier *via* substitution of Au metal contact with metals with higher work functions such as Pd and Pt, and through intensifying the build-in electric field *via* reducing the lateral scale of 2D channel.[38-40] Our results show that the well-designed device architecture proposed in this work are suitable for high performance self-powered optoelectronics devices, especially for the ultrafast photodetection.

METHODS

Device Fabrication: The devices presented in this work were fabricated using a conventional dry transfer method with a polydimethylsiloxane (PDMS) carrier. First, the SiO_2/Si substrate was cleaned with isopropanol, acetone, ethanol and deionized water in sequence. Few-layer graphene nanosheets were exfoliated onto the substrate. Then the InSe nanosheets were exfoliated onto a flexible polyethylene terephthalate (PET) substrate coated with a PDMS thin film. Next, the selected InSe nanosheet was transferred onto the graphene by using optical microscope and a homemade aligned transfer system. Lastly, two Au electrodes were fabricated using the conventional photolithographic techniques. Notably, the Au metal contacts were deposited with a ultra-slow rate (< 0.3 Å/s) to realize vdWs contact by avoiding damage of the underlying InSe and Gr layered materials.[38]

Device Characterization: The morphology of device was studied with an optical microscope (Olympus BX41) and a scanning probe microscope (SPM, Bruker Dimension Icon). The structure of InSe samples were identified with TEM (Tacnai-G2 F30). Raman and PL spectra

were carried out using a micro-Raman spectrometer system (HORIBA, HR800) equipped with 532 and 638 nm laser sources. For transient PL spectra measurement, a 375 nm pulsed laser was used as the light source.

Device Measurements: The electrical and optoelectronic performances were analyzed with a xenon lamp, monochromator (Zolix, Omni-λ300i), and a semiconductor characterization analyzer (Keithley, 4200-PA SCS). For the current noise measurement, a lock-in amplifier (Stanford Research System, SR865) and a low noise preamplifier (DL Instruments, DL1211) were used to record the noise currents. The device was positioned into a dark probe station (Lakeshore) to reduce the electromagnetic interference from the external environment during the tests. For the response time measurement, a pulse 532 nm laser (Spectra-Physic, Evolution-X) with a pulse width of 8 ns and a frequency of 2 kHz was used as the excitation light source, and an oscilloscope (Keysight, MSO-X 3104T) samping at 1 GS/s with 50 Ω input resistance was used to test the transient photocurrent signals. The voltage bias applied to the device was set to be 0 V. The scanning photocurrent microscopy was achieved by a modulated laser beam (520 nm with a frequency of 333 Hz) scanning over the device utilizing a scanning micro-motion platform (Thorlabs GVS212). The lock-in technique (Signal Recovery model 7270) was employed to amplify the obtained photocurrent signals. The light power density was measured using a power meter (OPHIR, VEGA ROHS). All the devices were measured at room temperature in an ambient environment.

ASSOCIATED CONTENT

The Supporting Information is available free of charge *via* the Internet at http://pubs.acs.org.

The details of materials characterizations, device electric simulation and characterizations with corresponding figures including:

S1. Device Architecture Design

S2. Device Structure Characterization

S3. van der Waals Contacts

S4. Highly Sensitive Self-Powered Photodetection

S5. Ultrafast Photoresponse Speed

S6. Working Mechanism (PDF)

AUTHOR INFORMATION

Corresponding Author

*E-mail: hupa@hit.edu.cn.

ORCID

Mingjin Dai: 0000-0001-6009-1715

Hongyu Chen: 0000-0002-3926-1959

Tianyou Zhai: 0000-0003-0985-4806

PingAn Hu: 0000-0003-3499-2733

Author Contributions

The authors declare no competing financial interest.

ACKNOWLEDGMENT

REFERENCES

(1)   Chen, S.; Shi, G. Q., Two-Dimensional Materials for Halide Perovskite-Based Optoelectronic Devices. *Adv. Mater.* **2017**, *29*, 1605448.

(2)   Shim, J.; Park, H. Y.; Kang, D. H.; Kim, J. O.; Jo, S. H.; Park, Y.; Park, J. H., Electronic and Optoelectronic Devices Based on Two-Dimensional Materials: From Fabrication to Application. *Adv. Electron. Mater.* **2017**, *3*, 1600364.

(3)   Wu, G.; Wang, X.; Chen, Y.; Wu, S.; Wu, B.; Jiang, Y.; Shen, H.; Lin, T.; Liu, Q.; Wang, X.; Zhou, P.; Zhang, S.; Hu, W.; Meng, X.; Chu, J.; Wang, J., MoTe$_2$ *p–n* Homojunctions Defined by Ferroelectric Polarization. *Adv. Mater.* **2020**, *32*, 1907937.

(4)   Tong, L.; Huang, X.; Wang, P.; Ye, L.; Peng, M.; An, L.; Sun, Q.; Zhang, Y.; Yang, G.; Li, Z.; Zhong, F.; Wang, F.; Wang, Y.; Motlag, M.; Wu, W.; Cheng, G. J.; Hu, W., Stable Mid-Infrared Polarization Imaging Based on Quasi-2D Tellurium at Room Temperature. *Nat. Commun.* **2020**, *11*, 2308.

(5)   Buscema, M. J.; Island, O.; Groenendijk, D. J.; Blanter, S. I.; Steele, G. A.; van der Zant, H. S. J.; Castellanos-Gomez, A., Photocurrent Generation with Two-Dimensional van der Waals Semiconductors. *Chem. Soc. Rev.* **2015**, *44*, 3691.

(6)   Chen, H. Y.; Liu, K. W.; Hu, L. F.; Al-Ghamdi, A. A.; Fang, X. S., New Concept Ultraviolet Photodetectors. *Mater. Today* **2015**, *18*, 493.

(7)   Konstantatos, G.; Badioli, M.; Gaudreau, L.; Osmond, J.; Bernechea, M.; de Arquer, F. P. G.; Gatti, F.; Koppens, F. H. L., Hybrid Graphene-Quantum Dot Phototransistors with Ultrahigh Gain. *Nat. Nanotechnol.* **2012**, *7*, 363.

(8)   Zhang, D. Y.; Gan, L.; Cao, Y.; Wang, Q.; Qi, L. M.; Guo, X. F., Understanding Charge Transfer at PbS-Decorated Graphene Surfaces toward a Tunable Photosensor. *Adv. Mater.* **2012**, *24*, 2715.

(9)   Gim, Y. S.; Lee, Y.; Kim, S.; Hao, S. Q.; Kang, M. S.; Yoo, W. J.; Kim, H.; Wolverton, C.; Cho, J. H., Organic Dye Graphene Hybrid Structures with Spectral Color Selectivity. *Adv. Funct. Mater.* **2016**, *26*, 6593.

(10)   Huang, Y. M.; Zheng, W.; Qiu, Y. F.; Hu, P. A., Effects of Organic Molecules with Different Structures and Absorption Bandwidth on Modulating Photoresponse of MoS_2 Photodetector. *ACS Appl. Mater. Interfaces* **2016**, *8*, 23362.

(11)   Lu, J. P.; Carvalho, A.; Liu, H. W.; Lim, S. X.; Neto, A. H. C.; Sow, C. H., Hybrid Bilayer WSe_2-$CH_3NH_3PbI_3$ Organolead Halide Perovskite as a High-Performance Photodetector. *Angew. Chem. Int. Ed.* **2016**, *55*, 11945.

(12)   Wang, L. M.; Zou, X. M.; Lin, J.; Jiang, J. Y.; Liu, Y.; Liu, X. Q.; Zhao, X. Y.; Liu, F.; Ho, J. C.; Liao, L., Perovskite/Black Phosphorus/MoS_2 Photogate Reversed Photodiodes with Ultrahigh Light On/Off Ratio and Fast Response. *ACS Nano* **2019**, *13*, 4804.

(13)   Chen, Z. F.; Li, X. M.; Wang, J. Q.; Tao, L.; Long, M. Z.; Liang, S. J.; Ang, L. K.; Shu, C.; Tsang, H. K.; Xu, J. B., Synergistic Effects of Plasmonics and Electron Trapping in Graphene Short-Wave Infrared Photodetectors with Ultrahigh Responsivity. *ACS Nano* **2017**, *11*, 430.

(14)   Lin, J. D.; Li, H.; Zhang, H.; Chen, W., Plasmonic Enhancement of Photocurrent in MoS_2 Field-Effect-Transistor. *Appl. Phys. Lett.* **2013**, *102*, 203109.

(15)   Zhang, X. K.; Liao, Q. L.; Kang, Z.; Liu, B. S.; Ou, Y.; Du, J. L.; Xiao, J. K.; Gao, L.; Shan, H. Y.; Luo, Y.; Fang, Z. Y.; Wang, P. D.; Sun, Z.; Zhang, Z.; Zhang, Y., Self-Healing Originated van der Waals Homojunctions with Strong Interlayer Coupling for High-Performance Photodiodes. *ACS Nano* **2019**, *13*, 3280.

(16)   Wu, W. Z.; Wang, Z. L., Piezotronics and Piezo-Phototronics for Adaptive Electronics and Optoelectronics. *Nat. Rev. Mater.* **2016**, *1*, 16031.

(17)   Lin, P.; Zhu, L. P.; Li, D.; Xu, L.; Pan, C. F.; Wang, Z. L., Piezo-Phototronic Effect for Enhanced Flexible MoS_2/WSe_2 van der Waals Photodiodes. *Adv. Funct. Mater.* **2018**, *28*, 1802849.

(18)   Ge, C.; Jin, K. J.; Lu, H. B.; Wang, C.; Zhao, G. M.; Zhang, L. L.; Yang, G. Z., Mechanisms for the Enhancement of the Lateral Photovoltage in Perovskite Heterostructures. *Solid State Commun.* **2010**, *150*, 2114.

(19)   Liu, C. H.; Chang, Y. C.; Lee, S.; Zhang, Y. Z.; Zhang, Y. F.; Norris, T. B.; Zhong, Z. H., ultrafast Lateral Photo-Dember Effect in Graphene Induced by Nonequilibrium Hot Carrier Dynamics. *Nano Lett.* **2015**, *15*, 4234.

(20)   Gao, A. Y.; Lai, J. W.; Wang, Y. J.; Zhu, Z.; Zeng, J. W.; Yu, G. L.; Wang, N. Z.; Chen, W. C.; Cao, T. J.; Hu, W. D.; Sun, D.; Chen, X. H.; Miao, F.; Shi, Y.; Wang, X. M., Observation of Ballistic Avalanche Phenomena in Nanoscale Vertical InSe/BP Heterostructures. *Nat. Nanotechnol.* **2019**, *14*, 217.

(21)   Jiang, J.; Ling, C. Y.; Xu, T.; Wang, W. H.; Niu, X. H.; Zafar, A.; Yan, Z. Z.; Wang, X. M.; You, Y. M.; Sun, L. T.; Lu, J. P.; Wang, J. L.; Ni, Z. H., Defect Engineering for Modulating the Trap States in 2D Photoconductors. *Adv. Mater.* **2018**, *30*, 1804332.

(22)   Zeng, J. P.; Meng, C. F.; Li, X. M.; Wu, Y.; Liu, S. T.; Zhou, H.; Wang, H.; Zeng, H. B., Interfacial-Tunneling-Effect-Enhanced $CsPbBr_3$ Photodetectors Featuring High Detectivity and Stability. *Adv. Funct. Mater.* **2019**, *51*, 1904461.

(23)   Vu, Q. A.; Lee, J. H.; Nguyen, V. L.; Shin, Y. S.; Lim, S. C.; Lee, K.; Heo, J.; Park, S.; Kim, K.; Lee, Y. H.; Yu, W. J., Tuning Carrier Tunneling in van der Waals Heterostructures for Ultrahigh Detectivity. *Nano Lett.* **2017**, *17*, 453.

(24) Wu, F.; Xia, H.; Sun, H. D.; Zhang, J. W.; Gong, F.; Wang, Z.; Chen, L.; Wang, P.; Long, M. S.; Wu, X.; Wang, J. L.; Ren, W. C.; Chen, X. S.; Lu, W.; Hu, W. D.; AsP/InSe van der Waals Tunneling Heterojunctions with Ultrahigh Reverse Rectification Ratio and High Photosensitivity. *Adv. Funct. Mater.* **2019**, *29*, 1900314.

(25) Zou, X. M.; Li, Y. Z.; Tang,;G. Q.; You, P.; Yan, F., Schottky Barrier-Controlled Black Phosphorus/Perovskite Phototransistors with Ultrahigh Sensitivity and Fast Response. *Small* **2019**, *15*, 1901004.

(26) Gibson, S. J.; van Kasteren, B.; Tekcan, B.; Cui, Y. C.; van Dam, D.; Haverkort, J. E. M.; Bakkers, E. P. A. M.; Reimer, M. E., Tapered InP Nanowire Arrays for Efficient Broadband High-Speed Single-Photon Detection. *Nat. Nanotechnol.* **2019**, *14*, 473.

(27) Wang, X.; Tian, W.; Liao, M. Y.; Bando, Y.; Golberg, D., Recent Advances in Solution-Processed Inorganic Nanofilm Photodetectors. *Chem. Soc. Rev.* **2014**, *43*, 1400.

(28) Li, C. L.; Cao, Q.; Wang, F. Z.; Xiao, Y. Q.; Li, Y. B.; Delaunay, J. J.; Zhu, H. W., Engineering Graphene and TMDs Based van der Waals Heterostructures for Photovoltaic and Photoelectrochemical Solar Energy Conversion. *Chem. Soc. Rev.* **2018**, *47*, 4981.

(29) Wang, L.; Huang, L.; Tan, W. C.; Feng, X. W.; Chen, L.; Huang, X.; Ang, K. W., 2D Photovoltaic Devices: Progress and Prospects. *Small Methods* **2018**, *2*, 1700294.

(30) Grundmann, M., *The Physics of Semiconductors,* Springer-Verlag Berlin Heidelberg: Springer, **2010**; *11*, 401-472.

(31) Tang, Y. C.; Wang, Z.; Wong, P.; Wu, F.; Wang, Y. M.; Chen, Y. F.; Wang, H. L.; Peng, M.; Shan, C. X.; Zhu, Z. H.; Qin, S. Q.; Hu, W. D., WSe$_2$ Photovoltaic Device Based on Intramolecular *p-n* Junction. *Small* **2019**, *15*, 1805545.

(32) Dai, M. J.; Chen, H. Y.; Feng, R.; Feng, W.; Hu, Y. X.; Yang, H. H.; Liu, G. B.; Chen, X. S.; Zhang, J.; Xu, C. Y.; Hu, P. A., A Dual-Band Multilayer InSe Self-Powered Photodetector with High Performance Induced by Surface Plasmon Resonance and Asymmetric Schottky Junction. *ACS Nano* **2018**, *12*, 8739.

(33) Dai, M.; Chen, H.; Wang, F.; Hu, Y.; Wei, S.; Zhang, J.; Wang, Z.; Zhai, T.; Hu, P., Robust Piezo-Phototronic Effect in Multilayer γ-InSe for High-Performance Self-Powered Flexible Photodetectors. *ACS Nano* **2019**, *13*, 7291.

(34) Groenendijk, D. J.; Buscema, M.; Steele, G. A.; de Vasconcellos, S. M.; Bratschitsch, R.; van der Zant, H. S. J.; Castellanos-Gomez, A., Photovoltaic and Photothermoelectric Effect in a Double-Gated WSe$_2$ Device. *Nano Lett.* **2014**, *14*, 5846.

(35) Wang, B.; Yang, S. X.; Wang, C.; Wu, M. H.; Huang, L.; Liu, Q.; Jiang, C. B.; Enhanced Current Rectification and Self-Powered Photoresponse in Multilayer *p*-MoTe$_2$/*n*-MoS$_2$ van der Waals Heterojunctions. *Nanoscale* **2017**, *9*, 10733.

(36) Wu, E. X.; Xie, Y.; Liu, Q. Z.; Hu, X. D.; Liu, J.; Zhang, D. H.; Zhou, C. W., Photoinduced Doping to Enable Tunable and High-Performance Anti-Ambipolar MoTe$_2$/MoS$_2$ Heterotransistors. *ACS Nano* **2019**, *13*, 5430.

(37) Wang, F.; Yin, L.; Wang, Z. X.; Xu, K.; Wang, F. M.; Shifa, T. A.; Huang, Y.; Jiang, C.; He, J., Configuration-Dependent Electrically Tunable van der Waals Heterostructures Based on MoTe$_2$/MoS$_2$. *Adv. Funct. Mater.* **2016**, *26*, 5499.

(38) Liu, Y.; Guo, J.; Zhu, E.; Liao, L.; Lee, S.; Ding, M.; Shakir, I.; Gambin, V.; Huang, Y.; Duan, X., Approaching the Schottky-Mott Limit in van der Waals Metal-Semiconductor Junctions. *Nature* **2018**, *557*, 696-700.

(39)   Wang, Y.; Kim, J.; Wu, R.; Martinez, J.; Song, X.; Yang, J.; Zhao, F.; Mkhoyan, K.; Jeong, H.; Chhowalla, M., van der Waals Contacts Between Three-Dimensional Metals and Two-Dimensional Semiconductors. *Nature* **2019**, *568*, 70-74.

(40)   Went, C.; Wong, J.; Jahelka, P.; Kelzenberg, M.; Biswas, S.; Hunt, M.; Carone, A.; Atwater, H., A New Metal Transfer Process for van der Waals Contacts to Vertical Schottky-Junction Transition Metal Dichalcogenide Photovoltaics. *Sci. Adv.* **2019,** *5*, eaax6061.

(41)   Wu, F., Li, Q.; Wang, P.; Xia, H.; Wang, Z.; Wang, Y.; Luo, M.; Chen, L.; Chen, F. S.; Miao, J. S.; Chen, X. S.; Lu, W.; Shan, C. X., A. L. Pan, X. Wu, W. C. Ren, D. Jariwala, W. D. Hu, High Efficiency and Fast van der Waals Hetero-Photodiodes with a Unilateral Depletion Region. *Nat. Commun.* **2019**, *10*, 4663.

(42)   Lopez-Sanchez, O.; Lembke, D.; Kayci, M.; Radenovic, A.; Kis, A., Ultrasensitive Photodetectors Based on Monolayer MoS2. *Nat. Nanotechnol.* **2013**, *8*, 497.

(43)   Milutinovic, A.; Lazarevic, Z. Z.; Jakovljevic, M.; Hadzic, B.; Petrovic, M.; Gilic, M.; Dobrowolski, W. D.; Romcevic, N. Z., Optical Properties of Layered III-VI Semiconductor Gamma-InSe:M (M=Mn, Fe, Co, Ni). *J. Phys. Chem. Solids* **2016**, *89*, 120.

(44)   Zhang, J.; Liu, J. J.; Wang, Z. L.; Wang, X. N.; Feng, W.; Zheng, W.; Cao, W. W.; Hu, P. A., Low-Temperature Growth of Large-Area Heteroatom-Doped Graphene Film. *Chem. Mater.* **2014**, *26*, 2460.

(45)   Wang, F.; Wang, Z. X.; Xu, K.; Wang, F. M.; Wang, Q. S.; Huang, Y.; Yin, L.; He, J., Tunable GaTe-MoS2 van der Waals *p-n* Junctions with Novel Optoelectronic Performance. *Nano Lett.* **2015**, *15*, 7558.

(46)   Mudd, G. W.; Svatek, S. A.; Hague, L.; Makarovsky, O.; Kudrynskyi, Z. R.; Mellor, C. J.; Beton, P. H.; Eaves, L.; Novoselov, K. S.; Kovalyuk, Z. D.; Vdovin, E. E.; Marsden, A. J.; Wilson, N. R.; Patane, A., High Broad-Band Photoresponsivity of Mechanically Formed InSe-Graphene van der Waals Heterostructures. *Adv. Mater.* **2015**, *27*, 3760.

(47)   Peng, B.; Yu, G. N.; Liu, X. F.; Liu, B.; Liang, X.; Bi, L.; Deng, L. J.; Sum, T. C.; Loh, K. P., ultrafast Charge Transfer in MoS2/WSe2 *p-n* Heterojunction. *2D Mater.* **2016**, *3*, 025020.

(48)   Zhou, X.; Hu, X. Z.; Zhou, S. S.; Song, H. Y.; Zhang, Q.; Pi, L. J.; Li, L.; Li, H. Q.; Lu, J. T.; Zhai, T. Y., Tunneling Diode Based on WSe2/SnS2 Heterostructure Incorporating High Detectivity and Responsivity. *Adv. Mater.* **2018**, *30*, 1703286.

(49)   Pan, S. D.; Ceballos, F.; Bellus, M. Z.; Zereshki, P.; Zhao, H., ultrafast Charge Transfer Between MoTe2 and MoS2 Monolayers. *2D Mater.* **2017**, *4*, 015033.

(50)   Bao, C. X.; Chen, Z. L.; Fang, Y. J.; Wei, H. T.; Deng, Y. H.; Xiao, X.; Li, L. L.; Huang, J. S., Low-Noise and Large-Linear-Dynamic-Range Photodetectors Based on Hybrid-Perovskite Thin-Single-Crystals. *Adv. Mater.* **2017**, *29*, 1703209.

(51)   Shen, L.; Fang, Y. J.; Wang, D.; Bai, Y.; Deng, Y. H.; Wang, M. M.; Lu, Y. F.; Huang, J. S., A Self-Powered, Sub-Nanosecond-Response Solution-Processed Hybrid Perovskite Photodetector for Time-Resolved Photoluminescence-Lifetime Detection. *Adv. Mater.* **2016**, *28*, 10794.

(52)   Georgiadou, D. G.; Lin, Y. H.; Lim, J.; Ratnasingham, S.; McLachlan, M. A.; Snaith, H. J.; Anthopoulos, T. D., High Responsivity and Response Speed Single-Layer Mixed-Cation Lead Mixed-Halide Perovskite Photodetectors Based on Nanogap Electrodes

Manufactured on Large-Area Rigid and Flexible Substrates. *Adv. Funct. Mater.* **2019**, *29*, 1901371.

(53)   Averine, S.; Sachot, R., Effects of High Space-Charge Fields on the Impulse Response of the Metal–Semiconductor–Metal Photodiode. *IEE Proc.: Optoelectron.* **2000**, *147*, 145.

(54)   Sun, Y. H.; Luo, S. L.; Zhao, X. G.; Biswas, K.; Li, S. L.; Zhang, L. J., InSe: A Two-Dimensional Material with Strong Interlayer Coupling. *Nanoscale* **2018**, *10*, 7991.

(55)   Feng, W.; Zheng, W.; Cao, W. W.; Hu, P. A., Back Gated Multilayer InSe Transistors with Enhanced Carrier Mobilities *via* the Suppression of Carrier Scattering from a Dielectric Interface. *Adv. Mater.* **2014**, *26*, 6587.

(56)   Kyazym-Zade, A. G.; Salmanov, V. M.; Guseinov, A. G.; Mamedov, R. M.; Salmanova, A. A.; Akhmedova, F. S., Special Features of the Optical Absorption and Photoconductivity of Indium Monoselenide upon Laser Excitation. *Russ. Phys. J* **2018**, *60*, 1680.

(57)   Yuksek, M.; Kurum, U.; Yaglioglu, H. G.; Elmali, A.; Ates, A., Nonlinear and Saturable Absorption Characteristics of Amorphous InSe Thin Films. *J. Appl. Phys.* **2010**, *107*, 033115.

(58)   Chen, Y.; Wang, X. D.; Wu, G. J.; Wang, Z.; Fang, H. H.; Lin, T.; Sun, S.; Shen, H.; Hu, W. D.; Wang, J. L.; Sun, J. L.; Meng, X. J.; Chu, J. H., High-Performance Photovoltaic Detector Based on $MoTe_2$/MoS_2 van der Waals Heterostructure. *Small* **2018**, *14*, 1703293.

(59)   Xie, Y.; Wu, E. X.; Zhang, J.; Hu, X. D.; Zhang, D. H.; Liu, J., Gate-Tunable Photodetection/Voltaic Device Based on BP/$MoTe_2$ Heterostructure. *ACS Appl. Mater. Interfaces* **2019**, *11*, 14215.

(60)   Lai, J. W.; Liu, X.; Ma, J. C.; Wang, Q. S.; Zhang, K. A.; Ren, X.; Liu, Y. A.; Gu, Q. Q.; Zhuo, X.; Lu, W.; Wu, Y.; Li, Y.; Feng, J.; Zhou, S. Y.; Chen, J. H.; Sun, D., Anisotropic Broadband Photoresponse of Layered Type-II Weyl Semimetal $MoTe_2$. *Adv. Mater.* **2018**, *30*, 1707152.

(61)   Yan, F. G.; Zhao, L. X.; Patane, A. L.; Hu, P. A.; Wei, X.; Luo, W. G.; Zhang, D.; Lv, Q. S.; Feng, Q.; Shen, C.; Chang, K.; Eaves, L.; Wang, K. Y., Fast, Multicolor Photodetection with Graphene-Contacted *p*-GaSe/*n*-InSe van der Waals Heterostructures. *Nanotechnology* **2017**, *28*, 27lt01.

(62)   Feng, W.; Jin, Z.; Yuan, J.; Zhang, J.; Jia, S.; Dong, L.; Yoon, J.; Zhou, L.; Vajtai, R. J.; Tour, M.; Ajayan, P. M.; Hu, P.; Lou, J., A Fast and Zero-Biased Photodetector Based on GaTe-InSe Vertical 2D *p-n* heterojunction. *2D Mater.* **2018**, *5*, 025008.

(63)   Zhao, S. W.; Wu, J. C.; Jin, K.; Ding, H. Y.; Li, T. S.; Wu, C. Z.; Pan, N.; Wang, X. P., Highly Polarized and Fast Photoresponse of Black Phosphorus-InSe Vertical *p-n* Heterojunctions. *Adv. Funct. Mater.* **2018**, *28*, 1802011.

ToC:
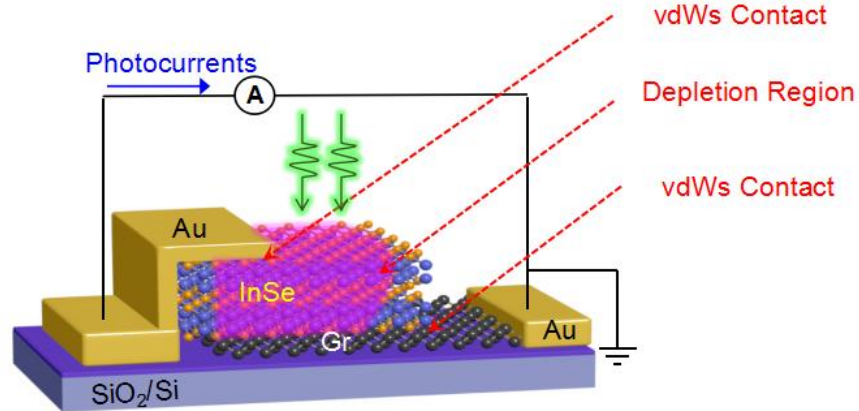
An ultrafast and sensitive self-powered photodetector based on two-dimensional semiconductor featuring a maximal latral self-limited depletion and a vertical fully depleted channe is realized with well-designed device architecture and formation of ideal Schottky or ohmic contacts. Driven by the vast photo-generated carriers and their ultrafast drift in the depletion region, a high responsivity of 365 mA/W, a detectivity over 10^{13} Jones, and a reduced response time of ~200 ns are achieved, indicating a pronounced application potential in ultrafast and sensitive self-powered photodetection.